Atmos. Chem. Phys. Discuss., 15, 14685–14732, 2015
www.atmos-chem-phys-discuss.net/15/14685/2015/
doi:10.5194/acpd-15-14685-2015

Atmospheric Chemistry and Physics Discussions

Reassessment of MIPAS age of air trends and variability

F. J. Haenel[1], G. P. Stiller[1], T. von Clarmann[1], B. Funke[2], E. Eckert[1], N. Glatthor[1], U. Grabowski[1], S. Kellmann[1], M. Kiefer[1], A. Linden[1], and T. Reddmann[1]

[1]Karlsruhe Institute of Technology, Institute for Meteorology and Climate Research, Karlsruhe, Germany
[2]Instituto de Astrofísica de Andalucía (CSIC), 18008 Granada, Spain

Received: 1 April 2015 – Accepted: 28 April 2015 – Published: 26 May 2015

Correspondence to: F. J. Haenel (florian.haenel@kit.edu)

Published by Copernicus Publications on behalf of the European Geosciences Union.

Abstract

A new and improved setup of the SF_6 retrieval together with a newly calibrated version of MIPAS-ENVISAT level 1b spectra (version 5, ESA data version 5.02/5.06) was used to obtain a new global SF_6-data set, covering the total observational period of MIPAS from July 2002 to April 2012 for the first time. Monthly and zonally averaged SF_6-profiles were converted into mean age of air using a tropospheric SF_6-reference curve. The obtained data set of age of air was compared to airborne and balloon-borne age of air measurements. The temporal evolution of mean age of air was then investigated in 10° latitude and 1–2 km altitude bins. A regression model consisting of a constant and a linear trend term, 2 proxies for the quasi-biennial oscillation variation, sinusoidal terms for the seasonal and semi-annual variation and overtones was fitted to the age of air time series. The annual cycle for particular regions in the stratosphere was investigated and compared to other studies. The age of air trend over the total MIPAS-period consisting of the linear term was assessed and compared to previous findings of Stiller et al. (2012). While the linear increase of mean age is confirmed to be positive for the Northern mid-latitudes and Southern polar middle stratosphere, differences are found in the Northern polar upper stratosphere, where the mean age is now found to increase as well. The magnitude of trends in the Northern mid-latitude middle stratosphere is slightly lower compared to the previous version and the trends fit remarkably well to the trend derived by Engel et al. (2009). Negative age of air trends found by Stiller et al. (2012) are confirmed for the lowermost tropical stratosphere and lowermost Southern mid-latitudinal stratosphere. Differences to the previous data versions occur in the middle tropical stratosphere around 25 km, where the trends are now negative. Overall, the new latitude–altitude distribution of trends appears to be less patchy and more coherent than the previous one. The new data provide evidence of an accelerating shallow branch of the Brewer–Dobson circulation, at least in the Southern Hemisphere. Finally the age of air decadal trends are compared to trends calculated with simulated SF_6 values by the Karlsruhe Simulation Model of the Middle

ACPD
15, 14685–14732, 2015

Atmosphere (KASIMA) and good agreement is found. The hemispheric asymmetry in the trends found in the MIPAS data are also indicated in the trends calculated with simulated SF_6 values by the KASIMA model.

1 Introduction

While it is widely accepted that climate change with enhanced greenhouse-gas abundances leads to a warming of the troposphere and a cooling of the stratosphere, the secondary effects, however, in particular on the global residual circulation in the stratosphere, the Brewer–Dobson-Circulation (BDC), are still an issue of current research (Butchart, 2014). A changing BDC will have large impact on the overall composition of the stratosphere, on the ozone budget and distribution (Shepherd, 2008; Li et al., 2009) and on the lifetimes of ozone-depleting substances such as CFCs (Butchart and Scaife, 2001; Douglass et al., 2008) and greenhouse gases. The mean age of air, which is the average transit time of an air parcel from the entry point of the stratosphere, the tropical tropopause, has become a measure for the strength of the BDC in particular for observational analysis (Hall and Plumb, 1994; Waugh and Hall, 2002). The mean age of air comprises both information on the speed of the advection and the amount of mixing and stirring exerted on the air parcel. Modern general circulation models (GCMs) and chemistry-climate models (CCMs) consistently simulate an acceleration of the BDC in a greenhouse gas-induced changing climate (Rind et al., 1990; Butchart and Scaife, 2001; Butchart et al., 2006; Austin and Li, 2006; Garcia and Randel, 2008; Li et al., 2008; Calvo and Garcia, 2009; McLandress and Shepherd, 2009; Butchart et al., 2010; Okamoto et al., 2011; Bunzel and Schmidt, 2013; Oberländer et al., 2013). So far, however, this expected speeding up of the BDC has not been confirmed by observations. Engel et al. (2009) provided a 30 year record of mean age of air derived from CO_2 and SF_6 balloon-borne measurements which showed a slight but insignificant increase of mean age over the years 1975–2005 for Northern mid-latitudes, which would indicate a decelerated BDC. Bönisch et al. (2011) reported an accelera-

ACPD
15, 14685–14732, 2015

tion of the shallow branch of the BDC for the time period 1979–2009, while they found an unchanged deep branch. Diallo et al. (2012) investigated the age of stratospheric air in the ERA-Interim reanalysis over the period 1989–2010 and stated that the shallow and the deep branch of the BDC may evolve differently. They found a negative and significant age of air trend in the lower stratosphere and a positive but insignificant trend in the middle stratosphere. Stiller et al. (2008, 2012) provided the first global data set on age of air derived from satellite SF_6 measurements. In their paper MIPAS-ENVISAT level 1b spectra of versions 3 and 4 were used to retrieve vertical profiles of SF_6 distributed over the whole globe for the time-period September 2002 to January 2010. Monthly zonal means were converted into mean age of air, from which decadal trends were inferred for latitude and altitude bins.

The derived age of air trends were found to be spatially inhomogeneous with regions of increasing mean age of air and regions of decreasing age of air. A hemispheric asymmetry was also found with SLIMCAT model calculations (Mahieu et al., 2014).

The work presented here is a continuation of the work of Stiller et al. (2012). An extended and improved SF_6 data set is provided on the basis of a newly calibrated version of MIPAS-ENVISAT level 1b spectra (version 5, ESA data version 5.02/5.06). This new global SF_6-data set for the first time covers the total MIPAS-period from July 2002 to April 2012.

The characteristics of the MIPAS instrument are presented in Sect. 2. The improvements on the retrieval setup are discussed in Sect. 3. The characteristics and morphology of the new global SF_6-data set and the resulting age of air data set are assessed in Sect. 4. Then the temporal development is investigated and compared with the previous findings (Sect. 5). In Sect. 6 MIPAS derived AoA trends are compared with trends calculated with simulated SF_6 values from the Karlsruhe Simulation Model of the Middle Atmosphere (KASIMA). Finally, in Sect. 7, we summarize the lessons learned about possible changes of the BDC.

ACPD
15, 14685–14732, 2015

2 MIPAS

MIPAS (Michelson Interferometer for Passive Atmospheric Sounding) is a Fourier transform infrared (FTIR) spectrometer aboard ENVISAT (Environmental Satellite, Fischer et al., 2000), which was launched in March 2002 by ESA (European Space Agency). ENVISAT's task was the permanent survey of the Earth's climate, the ocean, the land surfaces and the Earth's ecosystem in general. ENVISAT was a polar orbiting sun-synchronous satellite in an orbit of approx. 800 km with an inclination of the orbit of 98°. The mission of ENVISAT was planned with a lifetime of 5 years. In 2004 the operation of the MIPAS instrument was interrupted due to a problem with the interferometer slide. The optical path difference was then reduced, implying a deterioration of the spectral resolution from 0.025 to 0.0625 cm^{-1}, and since 2005 MIPAS was operational again in this mode. The first phase of the mission (2002–2004) is usually referred to as the MIPAS full resolution (FR) period, while the second phase is called the reduced resolution (RR) period. ENVISAT kept on sending data until April 2012, when ESA lost contact to ENVISAT.

MIPAS was designed for the detection of mid-infrared limb emission spectra in the middle and upper atmosphere. It observed a wide spectral interval ranging from 4.15 to 14.6 µm with high spectral resolution (Fischer et al., 2008). The atmospheric spectra were inverted into vertical profiles of atmospheric pressure, temperature and volume mixing ratios (vmrs) of at least 30 trace constituents. This allows studies of stratospheric chemistry and dynamics, stratosphere-troposphere exchange, chemistry and physics of the upper troposphere, chemistry and physics of the upper atmosphere, as well as climatologies and weather forecasting. One advantage of MIPAS was that as a limb emission instrument as opposed to a solar occultation instrument, it could measure globally and during day and night.

Because of the long optical path through the atmospheric layers, MIPAS could also detect trace gases with very low mixing ratios. Vertical information was gained by scanning the atmosphere at different elevation angles with different tangent altitudes. MIPAS

ACPD
15, 14685–14732, 2015

could observe atmospheric parameters in the altitude range from 5 to 160 km with minimum and maximum steps of 1 and 8 km, respectively (Fischer et al., 2008).

3 Improvement of the retrieval of SF_6 mixing ratios

Data processing relies on constrained least squares fitting using the Tikhonov (Tikhonov, 1963) regularization approach. Further details of the MIPAS data processor used are described in von Clarmann et al. (2003, 2009). Information on temperature and line of sight, as well as the spectral shift was taken from preceding MIPAS retrievals performed prior to SF_6 in the sequential retrieval chain.

While the retrieval of SF_6 by Stiller et al. (2012) relied on ESA version 4.61/4.62 and 4.67 calibrated radiance spectra, we have used version 5.02/5.06 spectra provided by ESA in the course of reprocessing of the data. These data are considered superior with respect to 4.61/4.62/4.67. Beyond this, the SF_6 retrieval setup has been improved over that used by Stiller et al. (2012). Improvements are related to the consideration of non-local thermodynamic equilibrium emission of interfering CO_2 lines, the treatment of interfering species in general, and the details of the joint-retrieval of the background continuum. The implementation of the altitude-dependence of the regularization strength has been slightly changed. The definition of the analysis window (941–952 cm^{-1}, see Fig. 1), the regularization strength of the inverse problem, and the spectroscopic database chosen remained unchanged since no improvements over the approach by Stiller et al. (2012) could be achieved with respect to these. Spectroscopic data were used from a dedicated MIPAS database for gases like H_2O, CO_2, O_3 and COF_2 (Flaud et al., 2003). For N_2O, NH_3, CFC-12 and SF_6 the spectroscopic database HITRAN2000 (Rothman et al., 2003) was used. Tests with varying regularization parameters did not lead to any retrieval improvements, i.e. the regularization strength chosen by Stiller et al. (2012) has been confirmed to be adequate. The new SF_6 data described and used here are version V5h_SF6_20 for the FR data product and V5r_SF6_222 and V5r_SF6_223 for the RR period. The latter two data

ACPD
15, 14685–14732, 2015

versions have no discernible differences; their different version numbers just reflect different sources of ECMWF meteorological analysis data used in the retrieval. In the FR V5h_SF6_20 data version the artefact of the previous version caused by radiance baseline oscillations in the level 1-data described in Stiller et al. (2008) is no longer an issue and has been totally overcome.

3.1 Non-local thermodynamic equilibrium

The Q branch of the ν_3 band of SF_6 at 947.9 cm^{-1} analysed here is strongly superimposed by the CO_2 laser band (00011 → 10001) at 947.74 cm^{-1} and lies just above the first hot band (01111 → 11101) line at 947.94 cm^{-1} (see Fig. 1). These CO_2 emission bands deviate from local thermodynamic equilibrium (LTE) in the middle atmosphere, particularly during daytime. Stiller et al. (2012) approximated the non-LTE effect by treating the CO_2 laser band and hot band emissions as emissions from different (non-CO_2) species and by fitting their "virtual abundances" along with the SF_6-retrieval. While these virtual abundances have no physical meaning, they helped to fairly well model the CO_2 laser band emission and to avoid related spectral residuals and error propagation. Contrary to that, our refined analysis relies on explicit modelling of the non-LTE emissions of the CO_2 laser and hot bands. In the course of a preceding CO retrieval (Funke et al., 2007), the vibrational temperatures of the CO_2 laser band and the hot band were calculated for the actual atmospheric conditions. Since the radiative transfer code used in our retrieval, the Karlsruhe Optimized and Precise Radiative Transfer Algorithm (KOPRA, Stiller, 2000; Stiller et al., 2002; Funke and Höpfner, 2000) supports calculation of non-LTE emissions, these could directly be used for the calculation of the laser band signal and hot band emissions. This improves considerably the description of the CO_2 emissions and reduces the residuals between the observed and modelled spectra, leading eventually to improved SF_6 results (compare residuals at the position of CO_2 lines in Fig. 2).

ACPD
15, 14685–14732, 2015

3.2 Interfering gases

Figure 1 shows the spectral window used for the SF_6 retrieval and the expected spectral contributions of contributing species for MIPAS reduced resolution at 20 km in mid-latitudes for July. The signature of the target species SF_6 (red solid line) is quite weak compared to some of the interfering species. Thus a careful treatment of the interfering species is essential to minimize related error propagation. Since for some of the interfering species no reliable a priori information on their abundances is available, these gases are jointly fitted along with SF_6. For other interferents, abundance information is available from preceding MIPAS retrievals; however inconsistent spectroscopic data or calibration inconsistencies in the SF_6 analysis window and the interferents' dedicated analysis windows can cause artefacts when the known abundances are used to model the contribution of these gases in the SF_6 analysis window. Thus, it is occasionally adequate to jointly fit these gases along with SF_6, too. Stiller et al. (2012) have used abundance information from climatologies or preceding MIPAS retrievals for all interfering species except for CO_2 and H_2O, which were fitted jointly along with SF_6. In the new retrieval scheme the trace gases COF_2 and ozone were additionally joint-fitted. This helped to minimize the residual of the fit and also removed a slight tilt of the residual in spectral space. For all gases a first order Tikhonov-type regularisation was chosen, which means that the slope of the profile was forced to some constraint, rather then forcing the profile towards an a priori profile as done in the Optimal Estimation approach. Usually the constant zero profile served as a priori profile and by this way oscillations in the profile are damped and the profile becomes smoother. In the following we present a gas-by-gas discussion of our treatment of all interfering species.

3.2.1 CO_2

CO_2 is the main contributing gas of all emitters in the SF_6 analysis window (microwindow) used (blue solid lines in Fig. 1). As mentioned above the maximum of the SF_6 spectral signature is just underneath of the wing of a CO_2 laser line. In order to get an

ACPD
15, 14685–14732, 2015

accurate value of the SF_6 mixing ratio from radiances emitted in the SF_6 microwindow, a very precise modelling of the CO_2 is crucial. We have used a non-LTE model to account for the CO_2 emissions in the middle atmosphere and fitted it jointly with SF_6. The first guess profile in the iterative procedure was taken from climatologies (Remedios et al., 2007).

3.2.2 H_2O

A water vapour signature is located near the SF_6 Q branch at 948.26 cm^{-1}, so a considerable information crosstalk is expected between the H_2O and the SF_6 signals. The water vapour profile resulting from the preceding retrieval in dedicated microwindows (prefit) was used as a priori and first guess profile for every geolocation. The regularization strength associated with H_2O was adjusted such that the correction with respect to the initial H_2O profile had about 1 to 1.5° of freedom. Basically the profiles have the shape of the prefit profile and only a shift of the prefit profile is allowed. The residual near the water vapour line was not reduced when the regularization for water vapour was relaxed. Variations of the regularization for water vapour or the choice of related a priori (constant zero or water prefit), did not have any discernible effect on the SF_6 retrieval.

3.2.3 COF_2

There is not much vertically resolved information contained on COF_2 in the microwindow, but fitting this trace gas jointly with the target species helped to minimize the residuals. A climatological profile served as a priori and first guess profile since there was no prefit of COF_2 available. The regularization was chosen relatively strong such that the resulting COF_2 profiles have about 1.5 to 3.5° of freedom.

ACPD
15, 14685–14732, 2015

3.2.4 O_3

Like COF_2, ozone is not much contributing to the signal in the used microwindow, but prefits from the ozone retrieval existed. Thus, the ozone prefits served as a priori and first guess profiles. Together with the joint fit of COF_2, the joint fit of ozone helped to remove a tilt in the residual. The regularization applied allowed the ozone profiles to have about 1.5 to 3.5° of freedom.

3.2.5 Further species

Profiles of N_2O, NH_3 and CFC-12 were imported from a climatological database (Remedios et al., 2007). Since the signals of these gases are small, related uncertainties are tolerable.

3.3 Background continuum and radiance offset

In the previous SF_6 retrieval by Stiller et al. (2012) background continuum radiation was considered up to an altitude of 33 km. In the atmosphere continuum radiation, i.e. radiation which is only varying very slightly in spectral space (in contrast to spectral lines), is emitted by clouds, dust or other aerosol particles. Also the sum of very far wings of spectral lines, no more accounted for by the line by line calculation, can contribute to the continuum radiation. In general it was assumed that a consideration of continuum radiation above 33 km was not necessary, particularly because there are no aerosol contributions expected above the Junge layer. However, it turned out that fitting continuum radiation up to higher altitudes (50 km) could eliminate an artefact in the retrieved SF_6 profile: while in the retrieval of Stiller et al. (2012) an unexplained local maximum in SF_6 occurred around 36 km in the tropics, this supposedly unphysical feature vanishes completely with the new continuum treatment. This provides evidence that there is additional continuum radiation in the atmosphere which if not accounted for leads to elevated SF_6 mixing ratios, since the SF_6 signature is also of broad band nature. The

ACPD
15, 14685–14732, 2015

approach of a joint fit of the continuum radiation up to higher altitudes also helped to improve other retrievals of other species. In addition, a recent paper pointed out that there is evidence of aerosol particles even above the Junge layer due to meteoric dust (Neely III et al., 2011). In our retrievals we also fit a constant radiance offset jointly, in order to account for a possible residual shift in radiance due to imperfect radiance calibration. This offset had to be strongly regularized in order to cope with the pronounced linear interdependence of the continuum and offset Jacobians.

3.4 Miscellaneous

The consideration of continuum up to higher altitudes allowed the usage of more upper tangent heights. While the previous retrieval setup only used the first 19 out of 27 tangent heights in MIPAS reduced resolution mode, the new setup incorporated information from measurements of 22 tangent heights. By this way more information could be gained at higher altitudes, i.e. the averaging kernel diagonals increased slightly at higher altitudes. In addition the root mean square (RMS) of the residuals in upper tangent heights decreased. Hence, with the new retrieval setup for the first time it made sense to include 22 tangents height instead of 19. The new mean SF_6 profiles contain more information in the altitude range 40–50 km, show more structure and depend less on the prior information there.

3.5 Discussion of the retrieval refinement

In Fig. 2 the residual between measured and simulated spectrum at tangent height 12 (approx. 23 km) of the final retrieval setup (upper panels) is shown while Fig. 2 (lower panels) show the respective residual of the previous setup. To reduce the noise measured and modelled spectra have been coadded over the period of 1 day. One can see that the residuals improved substantially. Especially the CO_2 lines and the water vapour line (compare with Fig. 1) are fitted much better and overall the RMS of the

ACPD
15, 14685–14732, 2015

residual has been reduced from about 1.8 to 1.0 nW $(cm^2\,sr\,cm^{-1})^{-1}$. Also a slight tilt of the residual in spectral space could be removed.

With the new retrieval setup the unphysical "nose", a local maximum, in the tropical SF_6 profiles at 36 km happened to disappear by considering the continuum above the standard altitude of 33 km up to an altitude of 50 km.

4 The new SF_6 database and age of air distributions

With the new retrieval setup, the complete set of nominal mode MIPAS data was processed and approx. 2.3 million SF_6 profiles have been retrieved. The profiles belong to geolocations that cover the whole globe and the full MIPAS period from July 2002 to April 2012 with several data gaps in between. The single profiles scatter a lot and the noise error is too large (in the order of 20 %) to provide useful age of air information from single profiles. But averaged profiles lead to meaningful SF_6-profiles. In Fig. 3 the time series of MIPAS SF_6 monthly zonal means at 25 km altitude is shown. SF_6 is increasing with time at almost all latitudes. Towards higher latitudes this increase is shifted in time, meaning that at higher latitudes the respective mixing ratios are reached at later times than in the tropics, as one would expect from the global circulation scheme. At high latitudes, especially in the Southern polar stratosphere seasonal influences can be identified. Every year in late austral winter to austral spring tongues with very low SF_6 mixing ratios appear in the Southern polar stratosphere. This can be explained by subsidence of very old air into the polar vortex, or even subsidence of SF_6 depleted air from the mesosphere. This effect is also indicated in the Northern polar stratosphere, but much less pronounced. This is explained by the fact that the polar vortex is less stable and pronounced in the Northern polar stratosphere and isolated subsidence inside the vortex does not occur that much.

The vertical resolution of the new SF_6 data is slightly degraded compared to the previous version to 4–6 at 20 km, 7–10 at 30 km and 12–18 at 40 km altitude due to the

ACPD
15, 14685–14732, 2015

inclusion of more gases in the fit, which was done to achieve a higher accuracy and less systematic errors.

4.1 Conversion of SF_6 into age of air

For the calculation of age of air (AoA) from SF_6 abundances a SF_6 reference curve is necessary. The theoretical concept of age of air as derived by Hall and Plumb (1994) requires the knowledge of SF_6 mixing ratios at the entry point into the stratosphere, i.e. the tropical tropopause region over a long period of time. As pointed out by Stiller et al. (2012) such a long term observational data set is not available. Only ground-based observations can provide the necessary reference data. However, transport times from the surface to the tropical tropopause are somewhat uncertain and can amount from days or even hours (to the top of convection) to weeks or months (to the top of the Tropical Tropopause Layer (TTL)). Using surface data as a reference can imply a high bias in this order of magnitude on the AoA data.

This has to be kept in mind when comparing MIPAS AoA distributions to model data, for which time zero is set by tropopause crossing of the air parcel.

We have constructed the SF_6 reference curve as described in Stiller et al. (2012) using NOAA/ESRL SF_6 data. For the period 1995 to November 2013 smoothed ground based global mean combined flask and in-situ data (Hall et al., 2011) is used while for times before 1995 a linear approximation from Hall et al. (2011) ($y = 0.125 + 0.215 \times (t - 1985)$) is applied. The reference curve is extended with a linear extrapolation until June 2014 to deal with MIPAS SF_6 values slightly higher than the reference values at that certain time that can occur sporadically due to their random errors.

The AoA is then calculated by simply mapping the measured SF_6 value on the reference curve and reading of the reference time. The time difference, the so called lag time approximates the AoA. According to Hall and Plumb (1994) this lag time is only equivalent to the mean age of air, if the used tracer is growing strictly linear, i.e. the reference curve has to be linear. Because our constructed reference curve appears to be slightly non-linear, a correction is applied. Within an iterative procedure the refer-

ACPD
15, 14685–14732, 2015

ence curve is convoluted with a typical age spectrum. More details of this non-linearity correction are discussed in Stiller et al. (2012).

SF_6 is a stable tracer in the stratosphere. However, it has a mesospheric sink. Every winter SF_6-depleted air from the mesosphere subsides into the polar vortex leading to "apparent ages" which are considerably larger than the true ages. This "overaging" is most pronounced in the polar vortices, where AoA derived from SF_6 can be greater by 2 or more years (Waugh and Hall, 2002). However, due to inmixing of some of the vortex air into mid-latitudes, the entire stratosphere is affected to a certain degree. This should be kept in mind when comparing AoA calculated from SF_6 abundances with AoA calculated from other tracers or model studies. The global effect of overaging is estimated at about 0.08 years per year of age for the Southern Hemisphere and 0.04 years per year of age for the Northern Hemisphere, respectively by Stiller et al. (2012).

4.2 Global distribution of AoA

The derived monthly zonal means of AoA have a precision in terms of the standard error of the means of 0.06–0.4 years for the reduced resolution period and of 0.08–0.5 years for the full resolution period. Most of the monthly means are composed of 500–800 single values, if fully occupied.

The global distribution of the newly derived AoA data set can be seen as average over all years for the four seasons in Fig. 4.

Highest AoA values occur in the polar stratosphere in hemispheric winter to spring being particularly high in the Southern Hemisphere. This again can be explained by intrusion and subsidence of old upper stratospheric and mesospheric air into the polar vortex. Due to the mesospheric SF_6 sink, this mesospheric air appears even older than it actually is.

The differences in the zonal monthly means of AoA to the previous data set, averaged over all years for the four seasons, are presented in Fig. 5. The main difference to the old data set is that the local minimum of AoA in the tropics around 36 km is no

ACPD
15, 14685–14732, 2015

more present in the new data set. This feature of the old data set has been proven to be a retrieval artefact, which was eliminated by a refined treatment of continuum radiation (see Sect. 3). This artefact triggered an oscillation in lower layers which are no longer present in the new data set. Above 40 km, the air is now found to be younger at almost all latitudes, which appears to be more realistic. The old data version was reported to have a possible high bias of up to 2 years above 35 km, most pronounced at the summer pole due to the simplified approach concerning the non-LTE treatment of interfering CO_2 lines (Stiller et al., 2008). The full non-LTE treatment used for the new data set has removed this systematic uncertainty. In addition, part of the lower AoA in the upper stratosphere is attributed to the revised regularization of the retrieval.

Among studies of AoA (e.g. Stiller et al., 2012; Diallo et al., 2012; SPARC CCMVal, 2010) it became a standard for validation of measured or modelled AoA to compare with earlier airborne measurements from the 1990s as published by Waugh and Hall (2002) and Hall et al. (1999). In Fig. 6 we compare the new MIPAS monthly zonal means of AoA with these airborne measurements. Figure 6 shows the latitudinal cross-section of the new MIPAS AoA at 20 km for selected months together with the total AoA range covered by all monthly mean data from MIPAS as derived from the minimum and maximum value for each latitude bin (shaded in grey), and the AoA derived from airborne measurements of SF_6 and CO_2. The AoA from CO_2 refers to CO_2 observations at the tropical tropopause, so it might exhibit a slight low bias compared to the SF_6 derived AoA measurements.

As with the previous version of MIPAS AoA discussed in Stiller et al. (2012) (Fig. 4), the agreement of MIPAS AoA with the earlier airborne measurements is excellent in the Northern and Southern mid-latitudes. Overall the comparison turns out to be quite similar to the one in Fig. 4 in Stiller et al. (2012): MIPAS AoA is higher in the tropics with an AoA of about 2 years at 20 km, maybe slightly lower than in the previous comparison. The negative peak of low MIPAS AoA at about 30° N is no more present in the new version of the figure and the spread of MIPAS AoA in the tropics is lower. At high latitudes MIPAS AoA is higher than the airborne observations, however, the error bars of

ACPD
15, 14685–14732, 2015

the airborne measurements still overlap with the range of the MIPAS observations. The spread of MIPAS data at high latitudes is very large, especially in the Southern polar stratosphere, and is in agreement with high amplitudes found in the seasonal cycle (see Sect. 5.2). By comparing the latitudinal cross-sections of MIPAS AoA with the aircraft data one has to keep in mind that these data were observed in the 1990s, whereas MIPAS AoA represent the decade from 2002 to 2012. We cannot expect that AoA estimates from different decades fit perfectly together, especially in the tropics where temperature changes have been reported (e.g. Randel et al., 2006). The AoA gradients at the subtropical mixing barriers are also smaller in the MIPAS data, which could be a hint to a weakening of the mixing barriers, as proposed by Stiller et al. (2012), which would also explain the higher ages in the tropics compared to the airborne data. In addition it should be noted that the airborne measurements do not represent a latitudinal cross-section at a given time, but a compilation of measurements from different years and seasons.

In Fig. 7 MIPAS AoA profiles are compared to airborne AoA profiles (in-situ CO_2 measurements by Boering et al., 1996; Andrews et al., 2001, in-situ SF_6 measurements by Ray et al., 1999 and air sample measurements by Harnisch et al., 1996) for the tropics (5° S), the Northern mid-latitudes (40° N) and the Northern high latitudes (65° N). In the tropics MIPAS AoA is older than in-situ CO_2 and SF_6 measurements at all altitudes as already observed at 20 km. In the Northern mid-latitudes the MIPAS profile fits excellently to the SF_6 in-situ data up to an altitude of 27 km and is older higher up. As expected, in-situ CO_2 measurements provide lower ages, and the AoA from SF_6 air samples by Harnisch et al. (1996) is younger, too. At Northern high latitudes, MIPAS age profiles only fit well to the SF_6 air samples taken from polar vortex air. To illustrate the high seasonality, monthly averaged MIPAS profiles are additionally shown with oldest ages found for January.

ACPD
15, 14685–14732, 2015

5 Observed temporal variability for the period July 2002 to April 2012

For the analysis of the temporal variability of the new AoA data set the same methods were applied as in Stiller et al. (2012), i.e. the following regression function was fitted to the data:

$$\text{age}(t) = a + bt + c_1 \text{qbo}_1(t) + d_1 \text{qbo}_2(t) + \sum_{n=2}^{9} \left(c_n \sin \frac{2\pi t}{l_n} + d_n \cos \frac{2\pi t}{l_n} \right) \quad (1)$$

where t is time, qbo_1 and qbo_2 are the quasi-biennial oscillation (QBO) indices, and the sum represents 8 sine and 8 cosine functions of the period length l_n. The period of the first two sine and cosine functions is 12 and 6 month, respectively, representing the seasonal and the semi-annual cycle. The other 6 terms have period lengths of 3, 4, 8, 9, 18 and 24 months and describe deviations of the temporal variation from a pure sine or cosine wave. Fitting sine and cosine of the same period length accounts for a possible phase shift of the oscillation. The terms qbo_1 and qbo_2 are the normalized Singapore winds at 30 and 50 hPa as provided by the Free University of Berlin via http://www.geo.fu-berlin.de/met/ag/strat/produkte/qbo/index.html. These QBO-proxies are approximately orthogonal such that their combination can emulate any QBO phase shift (Kyrölä et al., 2010). For the fit of the coefficients a, b, $c_1, \ldots, c_9$, $d_1, \ldots, d_9$ to the data, the method of von Clarmann et al. (2010) is used, which considers the full error covariance matrix of mean age data $\mathbf{S}_m$ with the squared standard errors of the means (SEM) of the monthly zonal means as the diagonal terms (Stiller et al., 2012).

5.1 Age of air trends without consideration of autocorrelation

First we discuss the timeseries analysis within the framework of descriptive statistics, i.e. without consideration of the autocorrelations in the residuals of the trend analysis. As a second step, the analysis is repeated within the framework of inductive statistics, where autocorrelated model errors have to be considered (Sect. 5.4).

ACPD
15, 14685–14732, 2015

Figure 8 shows an example of the fit of our regression model (in orange) to MIPAS monthly zonal mean data (in blue). The derived linear trend is illustrated in orange. The fit considers a potential bias of the two MIPAS measurement periods (dashed orange line) as described in von Clarmann et al. (2010). Coloured squares indicate the measurements of Engel et al. (2009) and the green dashed line represents their estimated trend. The diagram underneath shows the residual of the fit. Such a fit is done for every 10°/1–2 km latitude–altitude bin.

The linear increase of AoA over the whole MIPAS-period derived from our regression analysis varies with altitude and latitude. The global view can be seen in Fig. 9 top panel. Red areas indicate increasing AoA, while blue regions indicate decreasing AoA. The distribution of trends in the latitude–altitude plane roughly confirms the mean trends of those obtained by Stiller et al. (2012) and their general morphology but looks more coherent and less patchy, meaning that regions of linear increase and decrease, respectively, are more contiguous. There are basically two regions of linear decrease: A large one consisting of the tropics between about 19 to 33 km and extending to the lowermost mid-latitudinal Southern stratosphere, and a smaller one consisting of the upper tropical troposphere extending to the lowermost stratosphere of mid-latitudes. These regions are surrounded by regions of AoA linear increase. Largest positive linear trends were observed in the polar regions. Compared to findings of Stiller et al. (2012) a positive linear increase of mean age is confirmed for the Northern mid-latitudes and Southern upper polar stratosphere, as well as for the Northern polar lowermost stratosphere. Negative age of air trends of Stiller et al. (2012) in the lowermost tropical stratosphere and lower Southern mid-latitudinal stratosphere are also confirmed. Differences are found in the Northern polar stratosphere, where the mean age is now increasing as well. In the tropical stratosphere the picture is now almost opposite to the previous data of Stiller et al. (2012) meaning that AoA is increasing where it used to be decreasing and vice versa. These changes are attributed to the more adequate treatment of the background continuum emission in the retrieval and the associated removal of the spurious SF_6 maximum and subsequent errors.

ACPD
15, 14685–14732, 2015

The uncertainties are rather small, even smaller than the ones derived by Stiller et al. (2012) (see Fig. 9, bottom panel), which could be a result of the longer time series, covering now the full MIPAS period, and the fact that the new AoA data set is less noisy than the previous one. The results are significant on the 2σ level for most of the altitude/latitude bins (see Fig. 9, upper panel). Hatched areas indicate where the trend is not significant.

The vertical profiles of AoA linear trends for every other latitude bin are shown in Fig. 10, top panel. Engel et al. (2009) derived a trend of AoA for 30 to 50° N of $+0.24 \pm 0.22$ yr per decade (1σ uncertainty level) for the 24 to 35 km altitude range. This trend together with its valid altitude range and its 2σ uncertainty is marked as big black cross in Fig. 10. For better illustration the same picture with the MIPAS linear trend profiles for the two relevant latitude bins is shown in Fig. 10, bottom panel. The MIPAS AoA trends of 30 to 40 and 40 to 50° N are slightly lower than in the previous version and match now impressively well with the trend estimated by Engel et al. (2009) in the 24 to 35 km altitude region. One has to keep in mind, that the trend derived by Engel et al. (2009) represents the time period 1975–2005, while MIPAS measured from 2002 to 2012. So there is only a small time overlap between the two trends. Still the agreement of both is remarkable. The MIPAS AoA trends for the latitude bins 30 to 40 and 40 to 50° N are significantly distinct from zero for almost all altitudes above 17 km even on the 2σ uncertainty level.

5.2 Annual cycle

Figure 11 shows the amplitudes and phases of the seasonal cycle, i.e. the amplitudes and phases of terms with period length 1 year determined with the regression model described above. As observed by Stiller et al. (2012), the amplitudes of the seasonal variation are strongest in the Southern polar stratosphere, which can be explained by regular intrusion of SF_6-depleted mesospheric air into the polar winter vortex, which leads to very old apparent ages. Over the year, the oldest AoA occurs there at the end of Southern hemispheric winter to spring, as expected, while the youngest air is

ACPD
15, 14685–14732, 2015

observed at the end of Southern summer to autumn. This process is also observed in the Northern Hemisphere, but with smaller amplitude (see also Funke et al., 2005).

The phase shift of half a year between below and above 25 km in the polar stratosphere reported by Stiller et al. (2012) is only visible between the upper stratosphere and the lowest latitude–altitude bin in both hemispheres in the new MIPAS data. Diallo et al. (2012) found polar stratospheric AoA above 25 km, with youngest air at the end of local winter to spring, to be in the opposite phase than in the lowermost extra-tropical stratosphere in their analysis of ERA Interim data. In the model analysis of Li et al. (2012) the maximum of AoA in the polar region in spring is also bounded to the lower stratosphere whereas the upper polar stratosphere exhibits younger age. This difference to MIPAS AoA can be explained by the different derivations of AoA in the respective studies: while in Diallo et al. (2012) AoA is explicitly calculated by backward trajectories of the air parcel, and in Li et al. (2012) the AoA is determined by the pulse tracer method, the MIPAS AoA is derived by SF_6 observations which exhibit an overaging when SF_6 depleted mesospheric air subsides into the polar stratosphere during winter. This overaging in the polar stratosphere during winter shifts the phase in the MIPAS data towards oldest air in polar midwinter, when subsidence of mesospheric air is strongest.

In the tropics and most parts of the Northern mid-latitudes the amplitude of the seasonal cycle is rather small, except for the mid-latitudes above 25 km in both hemispheres, where also higher amplitudes can be found. The overall distribution of amplitudes is consistent to the one in Stiller et al. (2012), but there are also some discernible differences: the band of high seasonal amplitudes in the Northern mid-latitudes is not visible anymore in the new data.

The extra-tropical Southern lowermost stratosphere (LMS) exhibits now a higher amplitude of the seasonal cycle. Hence, now both hemispheres show enhanced seasonal amplitudes in the extra-tropical LMS, which are tentatively attributed to the seasonality of the permeability of the subtropical mixing barriers (the subtropical jet) (Stiller et al., 2012) and flooding of this region with old vortex air after the vortex breakdown at the

ACPD
15, 14685–14732, 2015

end of winter and spring. Consistently Diallo et al. (2012) found high amplitudes of the seasonal cycle in the Southern and Northern extra-tropical LMS. Most parts of both the Southern and Northern extra-tropical LMS reach their maximum in AoA in local spring in the MIPAS data set as well as in the analysis by Diallo et al. (2012). This hemispheric symmetry is a feature of the new MIPAS data set. Bönisch et al. (2009) found oldest AoA in the Northern LMS in April and youngest in October with in-situ measurements of SF_6 and CO_2 during the SPURT aircraft campaigns. MIPAS observed youngest air in hemispheric late summer to autumn when the mixing barrier in the subtropics is weakest and young air from the tropics is injected in this region, also referred to as "flushing" of the LMS (Hegglin and Shepherd, 2007). Also cross-tropopause isentropic mixing from the tropical troposphere in the extra-tropical LMS is enhanced during summer-early autumn when the subtropical jet is weak (Chen, 1995).

Model results of Li et al. (2012) of the seasonal variation of AoA also agree with MIPAS in the extra-tropical LMS.

In the Northern subtropical lower stratosphere an abrupt meridional phase shift of almost half a year occurs, which means that these air masses are well isolated by the subtropical jet. Equatorwards the air is oldest in summer, when the subtropical mixing barrier and the BDC are weakest and older air from the extra-tropics is mixed in. This process is also indicated in the Southern Hemisphere and these opposite phases between the subtropics and the extra-tropics are also observed in the model results of Li et al. (2012).

In the model simulation of Li et al. (2012) a vertical phase shift in the subtropics above 450 K (approx. 20 km) occurs. An indication of this phase shift is also visible in the MIPAS data, when the month of minimum age observed changes vertically from late winter to autumn in the Northern subtropics at 20 km.

In the mid-latitudinal middle and upper stratosphere the air is youngest in local winter, when, according to the known seasonality of the Brewer–Dobson-Circulation, younger air is brought to higher latitudes more efficiently. The mixing barriers are partially visible by abrupt phase shifts in the month of minimum and maximum age, respectively:

ACPD
15, 14685–14732, 2015

air masses in the polar vortex are well isolated from the rest of the hemisphere. The subtropical mixing barrier is visible in the Northern lower stratosphere at 30° N and is indicated in the upper stratosphere only in the plot of maximum age of Fig. 11. In the Southern Hemisphere the abrupt phase shifts seem to occur at 50–60° S and at 10–20° S.

In the tropics below approx. 28 km air is youngest in boreal winter, even in the Southern Hemisphere (except for altitude–latitude-bins below 20 km). The hemispheric difference is lower than expected, which was also noticed by Stiller et al. (2012). However, this minimum in AoA in the Southern tropics occurs approx. 2 month later in the new MIPAS data. In the Northern Hemisphere air is oldest in late summer, while it is oldest in austral spring to early summer in the Southern Hemisphere. Furthermore this maximum in AoA in the Southern tropics occurs 2 month earlier in the new MIPAS data set compared to the previous one.

In summary, apart from the mentioned differences, no substantial differences in the patterns of the months of maximum or minimum age, respectively, representing the phase of the seasonal variation, were found in the new data compared to the previous by Stiller et al. (2012). Thus, their respective conclusions remain valid in the light of the new data.

5.3 QBO influence

The amplitude of the QBO signal in AoA is shown in Fig. 12 for all latitudes and altitudes under assessment. High amplitudes are found not only in the tropics but also in the upper stratosphere of mid-latitudes, whereas highest amplitudes were found in the upper polar stratosphere. We also find high amplitudes in the Northern lowermost stratosphere. Overall the QBO influence seems to be more pronounced in the Southern Hemisphere above 25 km.

ACPD
15, 14685–14732, 2015

5.4 Impact of empirical errors and autocorrelation

As described in Stiller et al. (2012) our regression model only accounts for the linear trend, several periodics and the QBO-terms. Other atmospheric variability especially from non-periodic events is not included in this model. This results in fit residuals which are considerably larger than the data errors represented by the covariance matrix $\mathbf{S}_m$, which includes only the standard errors of the monthly means and the correlated terms to account for the possibly bias between the MIPAS data subsets (von Clarmann et al., 2010). Therefore the χ^2_{reduced} of the fit with

$$\chi^2_{\text{reduced}} = \frac{(\boldsymbol{age}_{\text{MIPAS}} - \boldsymbol{age}_{\text{modelled}})^{\mathrm{T}} \mathbf{S}_m^{-1} (\boldsymbol{age}_{\text{MIPAS}} - \boldsymbol{age}_{\text{modelled}})}{m - n} \quad (2)$$

exceeds the value of unity in most cases, where $\boldsymbol{age}_{\text{MIPAS}}$ and $\boldsymbol{age}_{\text{modelled}}$ are the data vectors containing the measured and modelled age values, respectively, and where m and n are the number of data pairs and the number of fitted coefficients, respectively (Stiller et al., 2012). In order to consider these model errors of the regression model, the autocorrelation of two adjacent data-points was estimated in a first step. In a second step the fit was rerun with the autocorrelation and a constant error term added to the covariance matrices. These additional terms in the covariance matrices were scaled within an iterative procedure, such that the resulting χ^2_{reduced} of the trend fit was close to unity. This iterative procedure is necessary because the additional autocorrelated error term changes the weight between the data points in the fit.

The result of the linear increase/decrease, which is referred to as "model-error corrected linear increase" in Stiller et al. (2012) is shown in Fig. 13. Compared with the respective Figure in Stiller et al. (2012) (Fig. 12) linear increase is again confirmed for the Northern mid-latitudes and the Southern polar middle stratosphere, whereas linear decrease is confirmed for the lowermost tropical stratosphere and lower and lowermost Southern mid-latitudinal stratosphere. Differences compared to Fig. 12 in Stiller et al. (2012) occur again in the tropics and in the Northern polar stratosphere, as well as in the upper Southern polar stratosphere.

ACPD
15, 14685–14732, 2015

The overall pattern of linear increase/decrease resembles a lot the pattern in the trend fit without consideration of autocorrelation and empirical errors (Fig. 9). The significance of most data bins is lower, as expected, due to the additional error. Significant features which appear in both approaches, with and without consideration of autocorrelation and empirical errors, are considered to be most reliable. By comparing Fig. 13 with Fig. 9 these features are the linear increase in the Southern and Northern upper polar stratosphere and in the Northern mid-latitudes as well as the linear decrease in the tropics and Southern subtropics and the Southern lower mid-latitudinal stratosphere. A clear asymmetry between both hemispheres is confirmed.

6 Comparison with model simulation

The MIPAS SF_6-based AoA trends are compared with trends derived from SF_6 distributions calculated with the Karlsruhe Simulation Model of the Middle Atmosphere (KASIMA), see Kouker et al. (1999); Ruhnke et al. (1999); Reddmann et al. (2001, 2010) for a description of the model and some applications. Here we used the model in the configuration as described in Reddmann et al. (2001), but with a T42/L63 configuration corresponding to about $2.84^\circ \times 2.84^\circ$ horizontal resolution and 63 vertical levels between 7 and 120 km. In addition, the model is nudged to ERA-Interim analyses below 1 hPa. SF_6 mixing ratio values were set at the lower boundary of the model in the troposphere using NOAA/ESRL data. Note, that the model includes the mesospheric loss of SF_6, which is implemented in the model according to Reddmann et al. (2001). Previously, Stiller et al. (2008) showed that only including mesospheric loss the apparent high mean age values in late polar stratospheric winter observed in MIPAS observations can be reproduced by the model simulations.

For the determination of the trend of SF_6 derived mean age of air in the model calculation, the SF_6 distributions were calculated on a pressure-latitude grid using 64 latitude bins. In each pressure-latitude bin monthly zonal averages of SF_6 were calculated together with their standard error of the mean. The vertical pressure coordinates

ACPD
15, 14685–14732, 2015

have been converted to geometrical altitudes assuming an isothermal atmosphere with a scale height H of 7 km ($z = -H\ln(p/p_0)$). Afterwards the monthly zonal means have been interpolated on the MIPAS altitude grid and binned in the MIPAS latitude bins. These regridded zonal SF_6 monthly means were sampled and converted to AoA in the same manner as it was done for the measured SF_6 values (see Sect. 4.1).

Figure 14 shows the distribution of age trends calculated with simulated SF_6 values from the KASIMA model in a latitude–altitude-plane with consideration of empirical errors and autocorrelations.

The model results agree remarkably well with the empirical AoA trends: positive decadal trends are found in the upper polar stratosphere in both hemispheres and at Northern mid-latitudes around 25 km while negative trends are found in the tropics and Southern subtropics as well as in the Southern lower and lowermost stratosphere of mid-latitudes and Southern polar region. The most pronounced negative trend is detected in the Southern tropics and subtropics around 25 km, as in the MIPAS measurements. At Northern mid-latitudes at about 30 km altitude a tongue of negative trend is modelled. While MIPAS detected still positive trends there, there is at least a local age trend minimum in this region in the MIPAS data. What is striking in Fig. 14 is the hemispheric asymmetry between significant negative trends in the Southern Hemisphere and significant positive trends in the Northern Hemisphere, which was also found in the MIPAS data. This hemispheric asymmetry was also noticed by Mahieu et al. (2014) with the SLIMCAT model. At high latitudes lower stratospheric trends are positive in the MIPAS but negative in the KASIMA data set. Differences in this region are most likely due to the "overaging" effect, which is more pronounced in the measured data because KASIMA underestimates polar winter subsidence.

7 Summary and conclusions

In this work the SF_6 retrieval setup for MIPAS ENVISAT spectra has been improved over the one developed by Stiller et al. (2012) and a newer version of ESA spectra (level

ACPD
15, 14685–14732, 2015

1b data, version 5.02/5.06) was used to retrieve global profiles of the trace gas SF_6. Monthly zonal means were converted in AoA using a tropospheric reference curve. The new AoA data set resembles roughly that of Stiller et al. (2012) but shows differences with respect to some details. Some spurious features of the old data set do no longer appear in the new data set. In particular, the new data set does not show the local AoA minimum at 36 km in the tropics, which was believed to be a retrieval artefact of the previous version and could be eliminated by a refined consideration of continuum radiation. A possible high bias of the old AoA data set above 40 km is removed as the air is considerably younger in this altitude region in the new data version.

The latitudinal cross-section of AoA at 20 km was compared to airborne observations from the 1990s and no substantial differences to the previous version of Stiller et al. (2012) were found. Apart from the tropics, most of the airborne data points overlap with their error bars with the range covered by the new MIPAS measurements. The comparison of AoA profiles with airborne measurements yields that in the tropics MIPAS AoA is older at all altitudes. At Northern mid-latitudes MIPAS agrees with most of SF_6 in-situ data whereas at high Northern latitudes MIPAS is again older, only the SF_6 air samples inside the polar vortex match with the MIPAS data.

The temporal variability of AoA over the 10 years of MIPAS measurements (2002–2012) was analysed by fitting a regression model to the AoA timeseries. The annual cycle in AoA of particular regions in the stratosphere was investigated and found to be in good agreement with other studies.

The derived AoA decadal trends show a pronounced hemispheric asymmetry above the lowermost stratosphere. The results of Stiller et al. (2012) were confirmed with respect to the typical values and the general morphology. The overall picture of linear increase/decrease in the latitude–altitude plane, however, is more contiguous and less patchy with the new data. Positive linear trends were confirmed for the Northern mid-latitudes and Southern polar middle stratosphere whereas negative trends were confirmed for the lowermost tropical stratosphere and lowermost Southern mid-latitudinal stratosphere. Differences to the previous data set occur in the Northern polar upper

ACPD
15, 14685–14732, 2015

stratosphere, where trends are now positive, and in the middle tropical stratosphere, where trends are now negative. The latter might be explained by the removal of the retrieval artefact which changed the shape of the AoA profile in the tropics considerably. The linear increase in the Southern and Northern polar stratosphere and in the Northern mid-latitudes can be considered as robust results. The significant positive trend in the Northern mid-latitudes supports the findings of Engel et al. (2009) and the inferred trends match impressively well with the estimated trend by Engel et al. (2009).

The refined MIPAS observations on AoA in this study do not corroborate the results of various model studies, which consistently predict a decreasing AoA for the whole stratosphere. However, our decadal trends cannot be compared to results from long-term model studies. Our comparison with the KASIMA model for the period 2002–2012 shows, that the linear increase in the upper polar stratosphere and in the Northern mid-latitudes can be reproduced in the model at least when data is sampled and analysed in the same manner as the MIPAS data.

Nevertheless this study finds a decreasing AoA trend in the tropics and in the lower and lowermost mid-latitudinal Southern stratosphere in agreement with long-term model studies, and hence supports the idea of an increasing shallow branch of the BDC, which was also proposed by Bönisch et al. (2011) and supported by Diallo et al. (2012), at least in the Southern Hemisphere.

Acknowledgements. This work was funded by the "CAWSES" priority programme of the German Research Foundation (DFG) under project STI 210/5-3 and by the German Federal Ministry of Education and Research (BMBF) within the "ROMIC" programme under project 01LG1221B.

E. Eckert was funded by the DFG project CL 319/2-1 (COLIBRI). We would like to acknowledge provision of MIPAS level-1b data by ESA and the SF_6 data from the NOAA/ESRL halocarbons in-situ programme. The authors also acknowledge support by Deutsche Forschungsgemeinschaft and Open Access Publishing Fund of Karlsruhe Institute of Technology.

ACPD
15, 14685–14732, 2015

The article processing charges for this open-access publication were covered by a Research Centre of the Helmholtz Association.

References

Andrews, A. E., Boering, K. A., Daube, B. C., Wofsy, S. C., Loewenstein, M., Jost, H., Podolske, J. R., Webster, C. R., Herman, R. L., Scott, D. C., Flesch, G. J., Moyer, E. J., Elkins, J. W., Dutton, G. S., Hurst, D. F., Moore, F. L., Ray, E. A., Romashkin, P. A., and Strahan, S. E.: Mean ages of stratospheric air derived from in situ observations of CO_2, CH_4, and N_2O, J. Geophys. Res., 106, 32295–32314, doi:10.1029/2001JD000465, 2001. 14700

Austin, J. and Li, F.: On the relationship between the strength of the Brewer–Dobson circulation and the age of stratospheric air, Geophys. Res. Lett., 33, L17807, doi:10.1029/2006GL026867, 2006. 14687

Boering, K. A., Wofsy, S. C., Daube, B. C., Schneider, H. R., Loewenstein, M., Podolske, J. R., and Conway, T. J.: Stratospheric mean ages and transport rates from observations of carbon dioxide and nitrous oxide, Science, 274, 1340–1343, doi:10.1126/science.274.5291.1340, 1996. 14700

Bönisch, H., Engel, A., Curtius, J., Birner, Th., and Hoor, P.: Quantifying transport into the lowermost stratosphere using simultaneous in-situ measurements of SF_6 and CO_2, Atmos. Chem. Phys., 9, 5905–5919, doi:10.5194/acp-9-5905-2009, 2009. 14705

Bönisch, H., Engel, A., Birner, Th., Hoor, P., Tarasick, D. W., and Ray, E. A.: On the structural changes in the Brewer–Dobson circulation after 2000, Atmos. Chem. Phys., 11, 3937–3948, doi:10.5194/acp-11-3937-2011, 2011. 14687, 14711

Bunzel, F. and Schmidt, H.: The brewer–dobson circulation in a changing climate: impact of the model configuration, J. Atmos. Sci., 70, 1437–1455, 2013. 14687

Butchart, N.: The Brewer–Dobson Circulation, Rev. Geophys., 52, 157–184, doi:10.1002/2013RG000448, 2014. 14687

Butchart, N. and Scaife, A. A.: Removal of chlorofluorocarbons by increased mass exchange between the stratosphere and troposphere in a changing climate, Nature, 410, 799–802, doi:10.1038/35071047, 2001. 14687

Butchart, N., Scaife, A. A., Bourqui, M., de Grandpre, J., Hare, S. H. E., Kettleborough, J., Langematz, U., Manzini, E., Sassi, F., Shibata, K., Shindell, D., and Sigmond, M.: Simulations

ACPD
15, 14685–14732, 2015

of anthropogenic change in the strength of the Brewer–Dobson circulation, Clim. Dynam., 27, 727–741, doi:10.1007/s00382-006-0162-4, 2006. 14687

Butchart, N., Cionni, I., Eyring, V., Shepherd, T. G., Waugh, D. W., Akiyoshi, H., Austin, J., Brühl, C., Chipperfield, M. P., Cordero, E., Dameris, M., Deckert, R., Dhomse, S., Frith, S. M., Garcia, R. R., Gettelman, A., Giorgetta, M. A., Kinnison, D. E., Li, F., Mancini, E., McLandress, C., Pawson, S., Pitari, G., Plummer, D. A., Rozanov, E., Sassi, F., Scinocca, J. F., Shibata, K., Steil, B., and Tian, W.: Chemistry–climate model simulations of twenty-first century stratospheric climate and circulation changes, J. Climate, 23, 5349–5374, 2010. 14687

Calvo, N. and Garcia, R. R.: Wave forcing of the tropical upwelling in the lower stratosphere under increasing concentrations of greenhouse gases, J. Atmos. Sci., 66, 3184–3196, 2009. 14687

Chen, P.: Isentropic cross-tropopause mass exchange in the extratropics, J. Geophys. Res.-Atmos., 100, 16661–16673, doi:10.1029/95JD01264, 1995. 14705

Diallo, M., Legras, B., and Chédin, A.: Age of stratospheric air in the ERA-Interim, Atmos. Chem. Phys., 12, 12133–12154, doi:10.5194/acp-12-12133-2012, 2012. 14688, 14699, 14704, 14705, 14711

Douglass, A. R., Stolarski, R. S., Schoeberl, M. R., Jackman, C. H., Gupta, M. L., Newman, P. A., Nielsen, J. E., and Fleming, E. L.: Relationship of loss, mean age of air and the distribution of CFCs to stratospheric circulation and implications for atmospheric lifetimes, J. Geophys. Res., 113, D14309, doi:10.1029/2007JD009575, 2008. 14687

Engel, A., Möbius, T., Bönisch, H., Schmidt, U., Heinz, R., Levin, I., Atlas, E., Aoki, S., Nakazawa, T., Sugawara, S., Moore, F., Hurst, D., Elkins, J., Schauffler, S., Andrews, A., and Boering, K.: Age of stratospheric air unchanged within uncertainties over the past 30 years, Nature Geosci., 2, 28–31, doi:10.1038/ngeo388, 2009. 14686, 14687, 14702, 14703, 14711, 14726, 14728

Fischer, H., Blom, C., Oelhaf, H., Carli, B., Carlotti, M., Delbouille, L., Ehhalt, D., Flaud, J.-M., Isaksen, I., López-Puertas, M., McElroy, C. T., and Zander, R.: Envisat-MIPAS, an instrument for atmospheric chemistry and climate research, European Space Agency-Report SP-1229, edited by: Readings C. and Harris R. A., ESA Publications Division, ESTEC, P.O. Box 299, 2200 AG Noordwijk, the Netherlands, 2000. 14689

Fischer, H., Birk, M., Blom, C., Carli, B., Carlotti, M., von Clarmann, T., Delbouille, L., Dudhia, A., Ehhalt, D., Endemann, M., Flaud, J. M., Gessner, R., Kleinert, A., Koopman, R., Langen, J., López-Puertas, M., Mosner, P., Nett, H., Oelhaf, H., Perron, G., Remedios, J.,

ACPD
15, 14685–14732, 2015

Ridolfi, M., Stiller, G., and Zander, R.: MIPAS: an instrument for atmospheric and climate research, Atmos. Chem. Phys., 8, 2151–2188, doi:10.5194/acp-8-2151-2008, 2008. 14689, 14690

Flaud, J.-M., Piccolo, C., Carli, B., Perrin, A., Coudert, L. H., Teffo, J.-L., and Brown, L. R.: Molecular line parameters for the MIPAS (Michelson Interferometer for Passive Atmospheric Sounding) experiment, Atmos. Oceanic Opt., 16, 172–182, 2003. 14690

Funke, B. and Höpfner, M.: Non-LTE and radiative transfer, in: The Karlsruhe Optimized and Precise Radiative Transfer Algorithm (KOPRA), edited by: Stiller, G. P., Wissenschaftliche Berichte FZKA 6487, Forschungszentrum Karlsruhe, Karlsruhe, 101–106, 2000. 14691

Funke, B., López-Puertas, M., Gil-López, S., von Clarmann, T., Stiller, G. P., Fischer, H., and Kellmann, S.: Downward transport of upper atmospheric NO_x into the polar stratosphere and lower mesosphere during the Antarctic 2003 and Arctic 2002/2003 winters, J. Geophys. Res., 110, D24308, doi:10.1029/2005JD006463, 2005. 14704

Funke, B., López-Puertas, M., Bermejo-Pantaleón, D., von Clarmann, T., Stiller, G. P., Höpfner, M., Grabowski, U., and Kaufmann, M.: Analysis of nonlocal thermodynamic equilibrium CO 4.7 µm fundamental, isotopic and hot band emissions measured by the Michelson Interferometer for Passive Atmospheric Sounding on Envisat, J. Geophys. Res., 112, D11305, doi:10.1029/2006JD007933, 2007. 14691

Garcia, R. R. and Randel, W. J.: Acceleration of the Brewer–Dobson circulation due to increases in greenhouse gases, J. Atmos. Sci., 65, 2731–2739, doi:10.1175/2008JAS2712.1, 2008. 14687

Hall, B. D., Dutton, G. S., Mondeel, D. J., Nance, J. D., Rigby, M., Butler, J. H., Moore, F. L., Hurst, D. F., and Elkins, J. W.: Improving measurements of SF_6 for the study of atmospheric transport and emissions, Atmos. Meas. Tech., 4, 2441–2451, doi:10.5194/amt-4-2441-2011, 2011. 14697

Hall, T. M. and Plumb, R. A.: Age as a diagnostic of stratospheric transport, J. Geophys. Res., 99, 1059–1070, 1994. 14687, 14697

Hall, T. M., Waugh, D. W., Boering, K. A., and Plumb, R. A.: Evaluation of transport in stratospheric models, J. Geophys. Res., 104, 18815–18839, 1999. 14699, 14724

Harnisch, J., Borchers, R., Fabian, P., and Maiss, M.: Tropospheric trends for CF_4 and C_2F_6 since 1982 derived from SF_6 dated stratosspheric air, Geophys. Res. Lett., 23, 1099–1102, 1996. 14700

ACPD
15, 14685–14732, 2015

Hegglin, M. I. and Shepherd, T. G.: O_3–N_2O correlations from the atmospheric chemistry experiment: revisiting a diagnostic of transport and chemistry in the stratosphere, J. Geophys. Res., 112, D19301, doi:10.1029/2006JD008281, 2007. 14705

Kouker, W., Offermann, D., Küll, V., Reddmann, T., Ruhnke, R., and Franzen, A.: Streamers observed by the CRISTA experiment and simulated in the KASIMA model, J. Geophys. Res., 104, 16405–16418, 1999. 14708

Kyrölä, E., Tamminen, J., Sofieva, V., Bertaux, J. L., Hauchecorne, A., Dalaudier, F., Fussen, D., Vanhellemont, F., Fanton d'Andon, O., Barrot, G., Guirlet, M., Fehr, T., and Saavedra de Miguel, L.: GOMOS O_3, NO_2, and NO_3 observations in 2002–2008, Atmos. Chem. Phys., 10, 7723–7738, doi:10.5194/acp-10-7723-2010, 2010. 14701

Li, F., Austin, J., and Wilson, J.: The strength of the brewer–dobson circulation in a changing climate: coupled chemistry–climate model simulations, J. Climate, 21, 40–57, 2008. 14687

Li, F., Stolarski, R. S., and Newman, P. A.: Stratospheric ozone in the post-CFC era, Atmos. Chem. Phys., 9, 2207–2213, doi:10.5194/acp-9-2207-2009, 2009. 14687

Li, F., Waugh, D. W., Douglass, A. R., Newman, P. A., Pawson, S., Stolarski, R. S., Strahan, S. E., and Nielsen, J. E.: Seasonal variations of stratospheric age spectra in the Goddard Earth Observing System Chemistry Climate Model (GEOSCCM), J. Geophys. Res.-Atmos., 117, D05134, doi:10.1029/2011JD016877, 2012. 14704, 14705

Mahieu, E., Chipperfield, M. P., Notholt, J., Reddmann, T., Anderson, J., Bernath, P. F., Blumenstock, T., Coffey, M. T., Dhomse, S. S., Feng, W., Franco, B., Froidevaux, L., Griffith, D. W. T., Hannigan, J. W., Hase, F., Hossaini, R., Jones, N. B., Morino, I., Murata, I., Nakajima, H., Palm, M., Paton-Walsh, C., Russell III, J. M., Schneider, M., Servais, C., Smale, D., and Walker, K. A.: Recent Northern Hemisphere stratospheric HCl increase due to atmospheric circulation changes, Nature, 515, 104–107, 2014. 14688, 14709

McLandress, C. and Shepherd, T. G.: Simulated anthropogenic changes in the Brewer–Dobson circulation, including its extension to high latitudes, J. Climate, 22, 1516–1540, doi:10.1175/2008JCLI2679.1, 2009. 14687

Neely III, R. R., English, J. M., Toon, O. B., Solomon, S., Mills, M., and Thayer, J. P.: Implications of extinction due to meteoritic smoke in the upper stratosphere, Geophys. Res. Lett., 38, L24808, doi:10.1029/2011GL049865, 2011. 14695

Oberländer, S., Langematz, U., and Meul, S.: Unraveling impact factors for future changes in the Brewer–Dobson circulation, J. Geophys. Res.-Atmos., 118, 10296–10312, doi:10.1002/jgrd.50775, 2013. 14687

ACPD
15, 14685–14732, 2015

Okamoto, K., Sato, K., and Akiyoshi, H.: A study on the formation and trend of the Brewer–Dobson circulation, J. Geophys. Res.-Atmos., 116, D10117, doi:10.1029/2010JD014953, 2011. 14687

Randel, W. J., Wu, F., Vömel, H., Nedoluha, G. E., and Forster, P.: Decreases in stratospheric water vapor after 2001: links to changes in the tropical tropopause and the Brewer–Dobson circulation, J. Geophys. Res., 111, D12312, doi:10.1029/2005JD006744, 2006. 14700

Ray, E. A., Moore, F. L., Elkins, J. W., Dutton, G. S., Fahey, D. W., Vömel, H., Oltmans, S. J., and Rosenlof, K. H.: Transport into the Northern Hemisphere lowermost stratosphere revealed by in situ tracer measurements, J. Geophys. Res., 104, 26565–26580, doi:10.1029/1999JD900323, 1999. 14700

Reddmann, T., Ruhnke, R., and Kouker, W.: Three–dimensional model simulations of SF_6 with mesospheric chemistry, J. Geophys. Res., 106, 14525–14537, doi:10.1029/2000JD900700, 2001. 14708

Reddmann, T., Ruhnke, R., Versick, S., and Kouker, W.: Modeling disturbed stratospheric chemistry during solar-induced NO_x enhancements observed with MIPAS/ENVISAT, J. Geophys. Res.-Atmos., 115, D00I11, doi:10.1029/2009JD012569, 2010. 14708

Remedios, J. J., Leigh, R. J., Waterfall, A. M., Moore, D. P., Sembhi, H., Parkes, I., Greenhough, J., Chipperfield, M.P., and Hauglustaine, D.: MIPAS reference atmospheres and comparisons to V4.61/V4.62 MIPAS level 2 geophysical data sets, Atmos. Chem. Phys. Discuss., 7, 9973–10017, doi:10.5194/acpd-7-9973-2007, 2007. 14693, 14694

Rind, D., Suozzo, R., Balachandran, N. K., and Prather, M. J.: Climate change and the middle atmosphere. part i: the doubled CO_2 climate, J. Atmos. Sci., 47, 465–494, 1990. 14687

Rothman, L. S., Barbe, A., Benner, D. C., Brown, L. R., Camy-Peyret, C., Carleer, M. R., Chance, K., Clerbaux, C., Dana, V., Devi, V. M., Fayt, A., Flaud, J.-M., Gamche, R. R., Goldman, A., Jacquemart, D., Jucks, K. W., Lafferty, W. J., Mandin, J.-Y., Massie, S. T., Nemtchinov, V., Newnham, D. A., Perrin, A., Rinsland, C. P., Schroeder, J., Smith, K. M., Smith, M. A. H., Tang, K., Toth, R. A., Vander Auwera, J., Varanasi, P., and Yoshino, K.: The HITRAN molecular spectroscopic database: edition of 2000 including updates through 2001, J. Quant. Spectrosc. Ra., 82, 5–44, doi:10.1016/S0022-4073(03)00146-8, 2003. 14690

Ruhnke, R., Kouker, W., and Reddmann, T.: The influence of the $OH + NO_2 + M$ reaction on the NO_y partitioning in the late Arctic winter 1992/1993 as studied with KASIMA, J. Geophys. Res., 104, 3755–3772, 1999. 14708

ACPD
15, 14685–14732, 2015

Shepherd, T. G.: Dynamics, stratospheric ozone, and climate change, Atmos. Ocean, 46, 117–138, doi:10.3137/ao.460106, 2008. 14687

SPARC CCMVal: Neu, J. and Strahan, S., Chapter 5. Transport, in: SPARC Report on the Evaluation of Chemistry-Climate Models, edited by: Eyring, V., Shepherd, T. G., and Waugh, D. W., SPARC Report No. 5, WCRP-132, WMO/TD-No. 1526, available at: http://www.atmosp.physics.utoronto.ca/SPARC, SPARC/WMO, Zurich, 2010. 14699

Stiller, G. P. (Ed.): The Karlsruhe Optimized and Precise Radiative Transfer Algorithm (KOPRA), vol. FZKA 6487 of Wissenschaftliche Berichte, Forschungszentrum Karlsruhe, 2000. 14691

Stiller, G. P., von Clarmann, T., Funke, B., Glatthor, N., Hase, F., Höpfner, M., and Linden, A.: Sensitivity of trace gas abundances retrievals from infrared limb emission spectra to simplifying approximations in radiative transfer modelling, J. Quant. Spectrosc. Ra., 72, 249–280, 2002. 14691

Stiller, G. P., von Clarmann, T., Höpfner, M., Glatthor, N., Grabowski, U., Kellmann, S., Kleinert, A., Linden, A., Milz, M., Reddmann, T., Steck, T., Fischer, H., Funke, B., López-Puertas, M., and Engel, A.: Global distribution of mean age of stratospheric air from MIPAS SF_6 measurements, Atmos. Chem. Phys., 8, 677–695, doi:10.5194/acp-8-677-2008, 2008. 14688, 14691, 14699, 14708

Stiller, G. P., von Clarmann, T., Haenel, F., Funke, B., Glatthor, N., Grabowski, U., Kellmann, S., Kiefer, M., Linden, A., Lossow, S., and López-Puertas, M.: Observed temporal evolution of global mean age of stratospheric air for the 2002 to 2010 period, Atmos. Chem. Phys., 12, 3311–3331, doi:10.5194/acp-12-3311-2012, 2012. 14686, 14688, 14690, 14691, 14692, 14694, 14697, 14698, 14699, 14700, 14701, 14702, 14703, 14704, 14706, 14707, 14709, 14710

Tikhonov, A.: On the solution of incorrectly stated problems and method of regularization, Dokl. Akad. Nauk. SSSR+, 151, 501–504, 1963. 14690

von Clarmann, T., Glatthor, N., Grabowski, U., Höpfner, M., Kellmann, S., Kiefer, M., Linden, A., Mengistu Tsidu, G., Milz, M., Steck, T., Stiller, G. P., Wang, D. Y., Fischer, H., Funke, B., Gil-López, S., and López-Puertas, M.: Retrieval of temperature and tangent altitude pointing from limb emission spectra recorded from space by the Michelson Interferometer for Passive Atmospheric Sounding (MIPAS), J. Geophys. Res., 108, 4736, doi:10.1029/2003JD003602, 2003. 14690

von Clarmann, T., Höpfner, M., Kellmann, S., Linden, A., Chauhan, S., Funke, B., Grabowski, U., Glatthor, N., Kiefer, M., Schieferdecker, T., Stiller, G. P., and Versick, S.: Retrieval of temper-

ACPD
15, 14685–14732, 2015

ature, H_2O, O_3, HNO_3, CH_4, N_2O, $ClONO_2$ and ClO from MIPAS reduced resolution nominal mode limb emission measurements, Atmos. Meas. Tech., 2, 159–175, doi:10.5194/amt-2-159-2009, 2009. 14690

von Clarmann, T., Stiller, G., Grabowski, U., Eckert, E., and Orphal, J.: Technical Note: Trend estimation from irregularly sampled, correlated data, Atmos. Chem. Phys., 10, 6737–6747, doi:10.5194/acp-10-6737-2010, 2010. 14701, 14702, 14707

Waugh, D. W. and Hall, T. M.: Age of stratospheric air: theory, observations, and models, Rev. Geophys., 40, 1010, doi:10.1029/2000RG000101, 2002. 14687, 14698, 14699, 14724

ACPD
15, 14685–14732, 2015

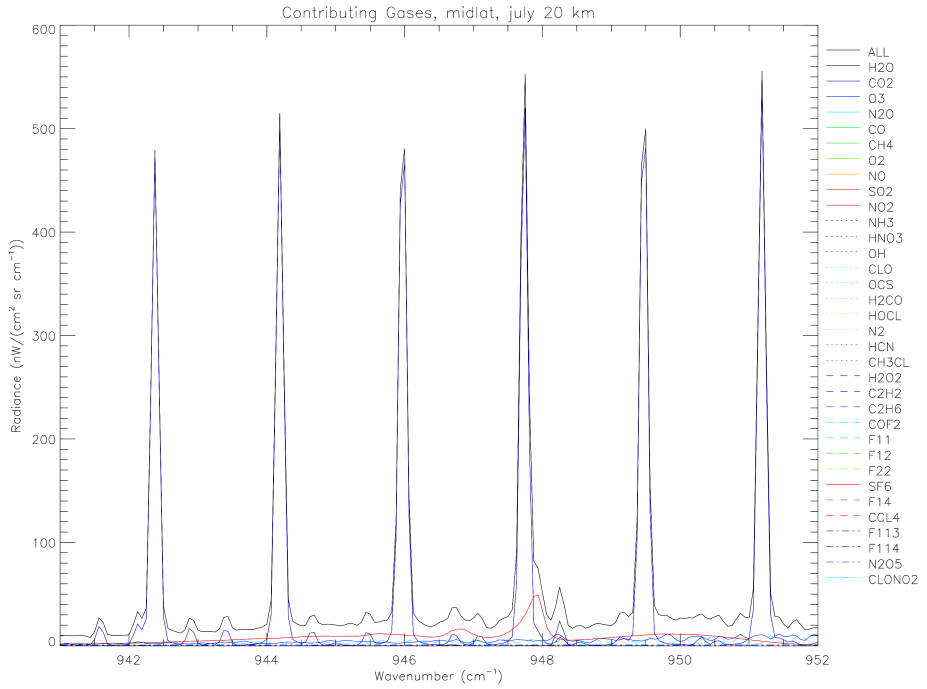

Figure 1. Contributing spectra in mid-latitudes in July at 20 km (low resolution) with the SF_6 signature in red.

ACPD
15, 14685–14732, 2015

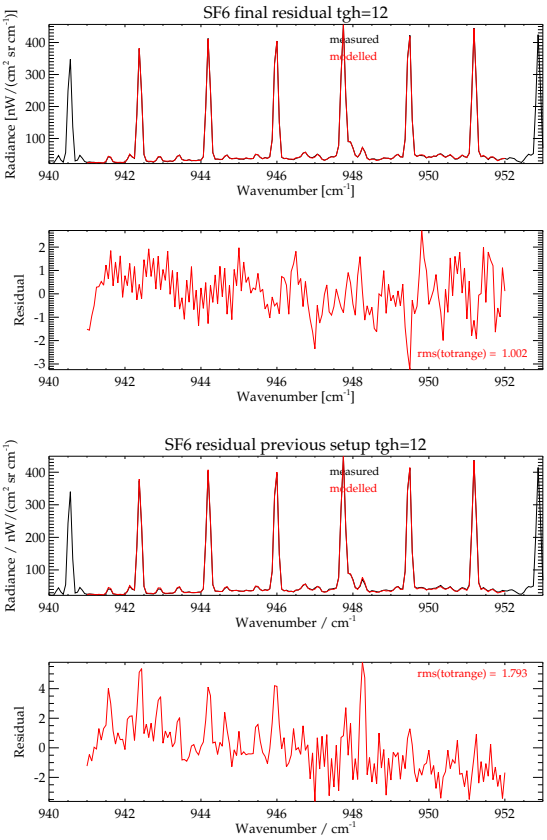

Figure 2. Coadded spectra (measured and modelled) and residuals for tangent height 12 (approx. 23 km) over one day for the final retrieval setup (upper panels) and for the the previous retrieval setup (lower panels).

ACPD
15, 14685–14732, 2015

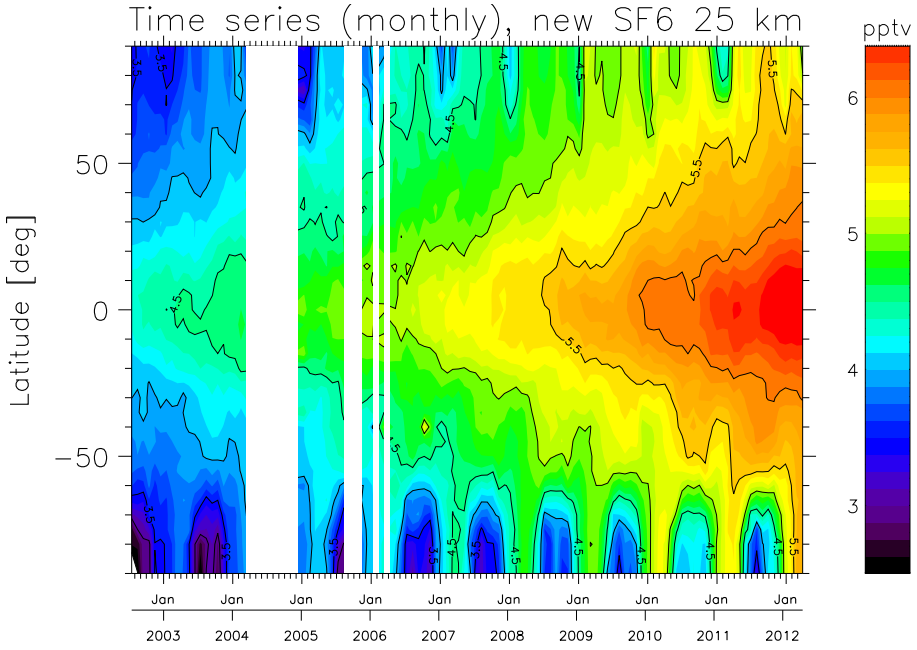

Figure 3. Timeseries of SF_6 monthly zonal means at 25 km.

ACPD
15, 14685–14732, 2015

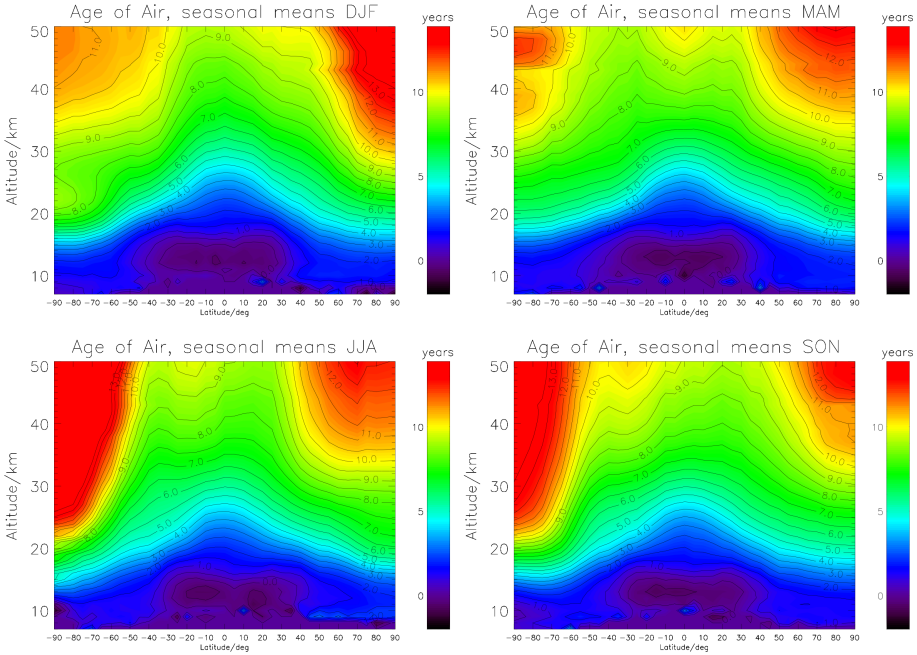

Figure 4. Zonal mean distribution of mean age of stratospheric air for the four seasons, derived by averaging MIPAS AoA data of all available years for the respective season.

ACPD
15, 14685–14732, 2015

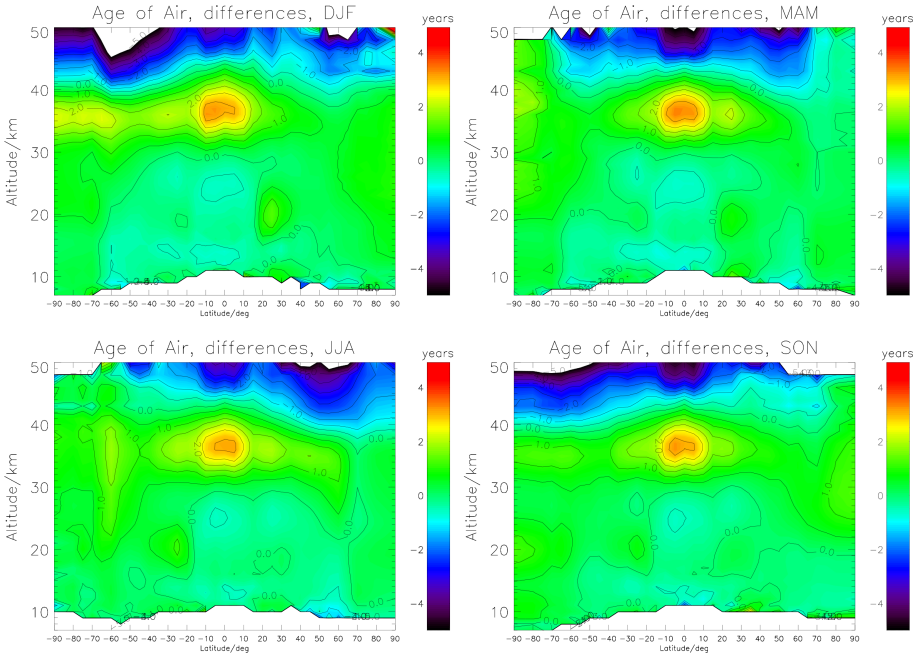

Figure 5. Differences of zonal seasonal mean distribution of mean age of stratospheric air to the previous data version averaged for the four seasons.

ACPD
15, 14685–14732, 2015

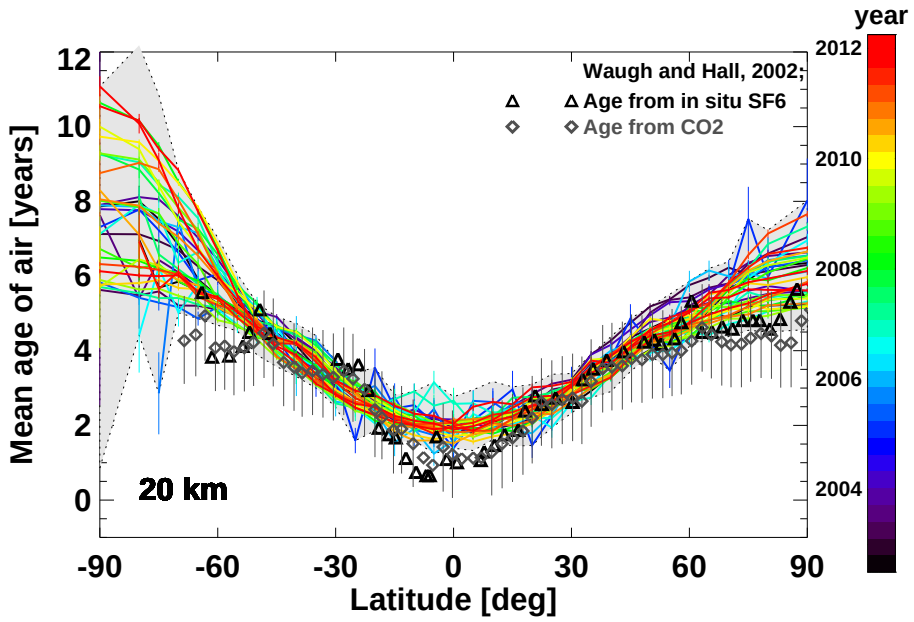

Figure 6. Comparison of MIPAS AoA latitude cross-sections at 20 km altitude (coloured curves and shaded area) with AoA derived from earlier airborne SF_6 (black triangles) and CO_2 measurements (grey diamonds with error bars) as published in Waugh and Hall (2002) and Hall et al. (1999). The shaded area represents the range of all MIPAS monthly mean AoA observations, while the coloured curves show AoA latitudinal dependence for every third month. The colour code provides the time of measurement.

ACPD
15, 14685–14732, 2015

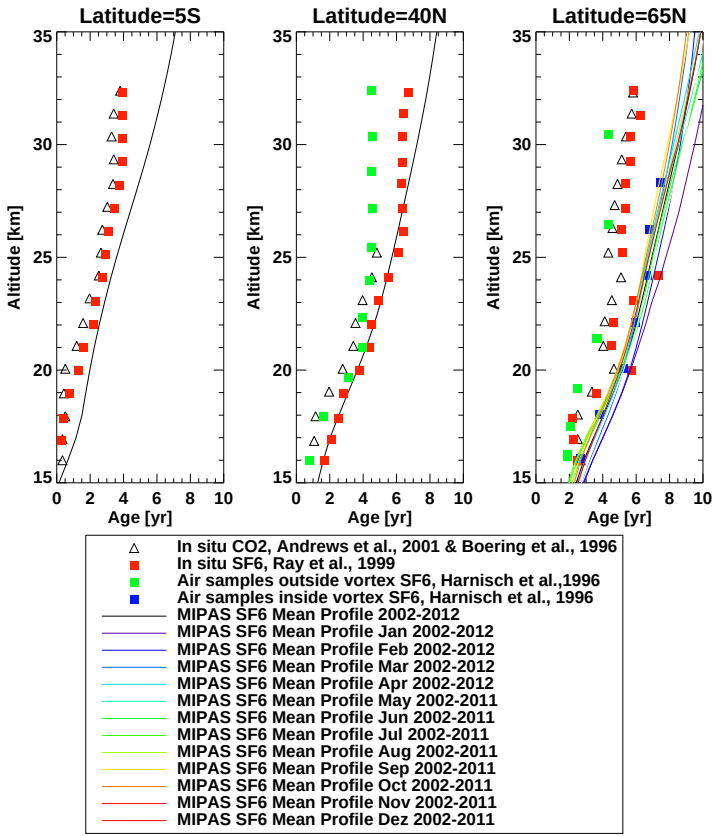

Figure 7. Comparison of MIPAS AoA profiles with airborne profiles of the 1990s for the tropics (5° S), the Northern mid-latitudes (40° N) and the Northern high latitudes (65° N).

ACPD
15, 14685–14732, 2015

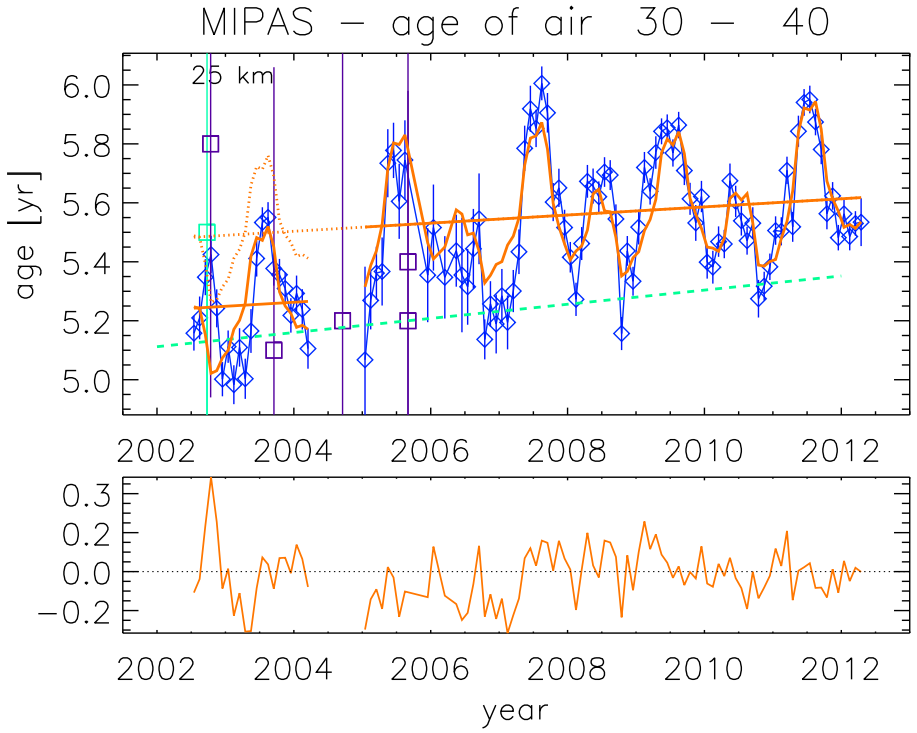

Figure 8. Example of the fit (in orange) of the regression model to MIPAS AoA monthly means (in blue) at 25 km for 30 to 40° N. The error bars represent the standard error of the mean (SEM). The orange line is the derived trend, squares represent the measurements by Engel et al. (2009) and green dashed line their estimated trend. Underneath the residual of the fit is shown.

ACPD
15, 14685–14732, 2015

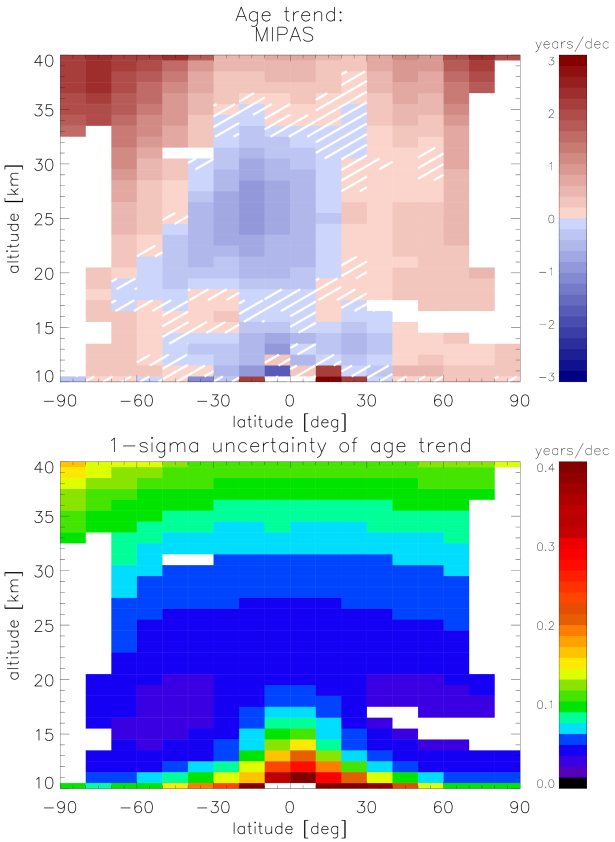

Figure 9. Altitude–latitude cross-sections of the MIPAS age of air linear increase/decrease over the years 2002 to 2012 (top), together with its 1σ uncertainties (bottom). White areas indicate where residuals between measurements and regression model get too large ($\chi^2 > 30$). Hatched areas indicate where the trend is not significant.

ACPD
15, 14685–14732, 2015

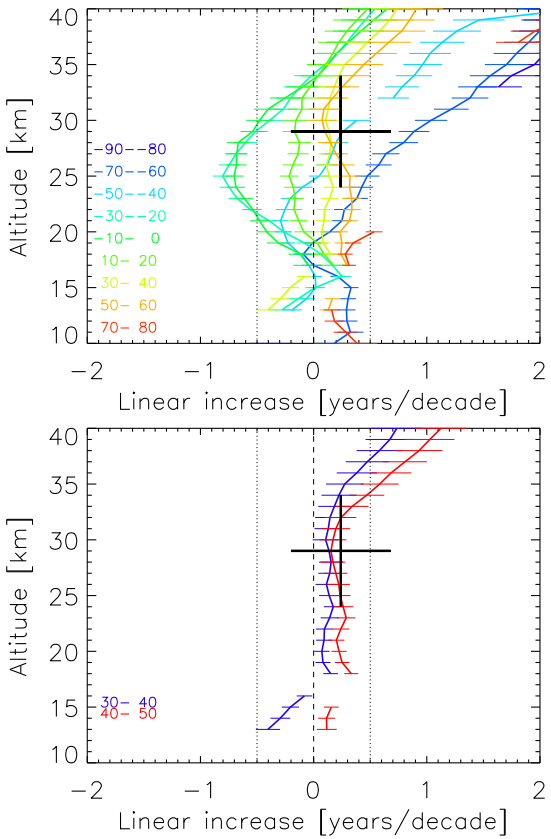

Figure 10. Vertical profiles of the age of air linear increase/decrease over the years 2002 to 2012 for example latitudes. Horizontal bars give the 2σ uncertainties of the linear variations. The 30 yr trend as derived by Engel et al. (2009) is also shown for comparison as a black cross indicating its valid altitude range and its 2σ-uncertainty.

ACPD
15, 14685–14732, 2015

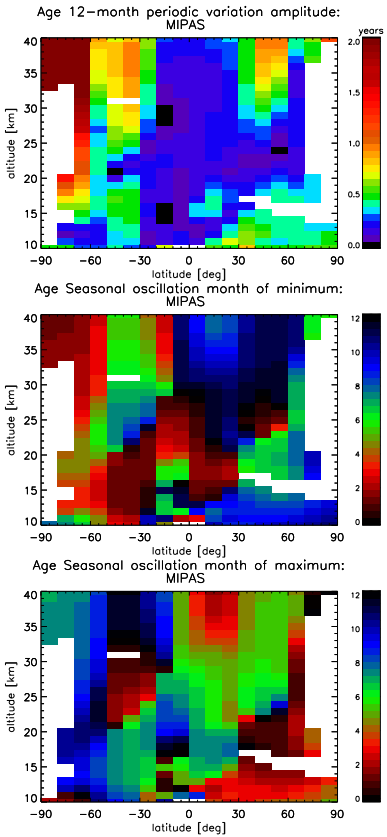

Figure 11. Altitude–latitude cross-sections of amplitudes (top) and month of the minimum (middle) and maximum (bottom) of the seasonal variation of mean age of air.

ACPD
15, 14685–14732, 2015

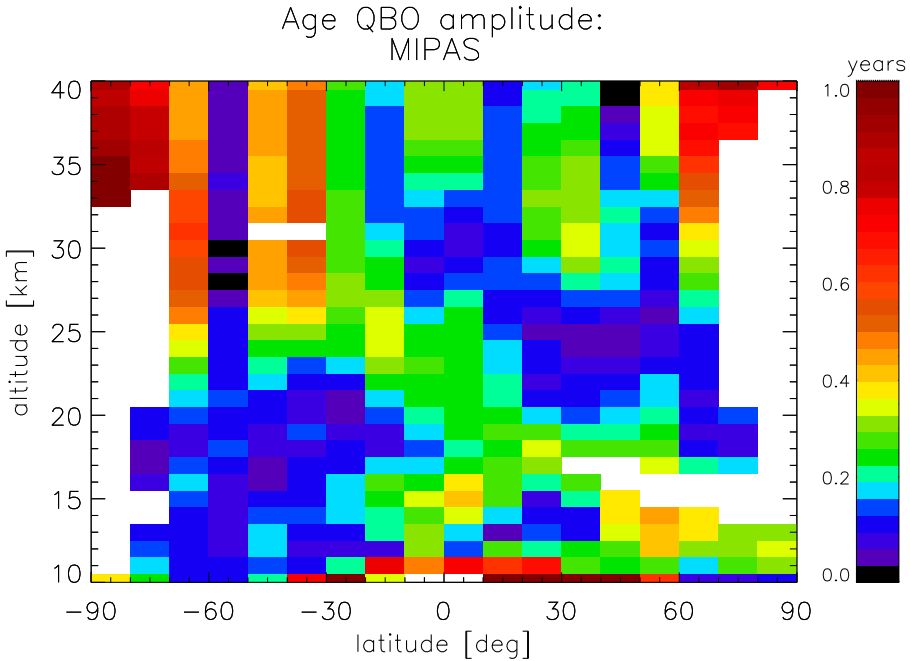

Figure 12. Altitude–latitude cross-sections of amplitudes of the QBO-variation of mean age of air.

ACPD
15, 14685–14732, 2015

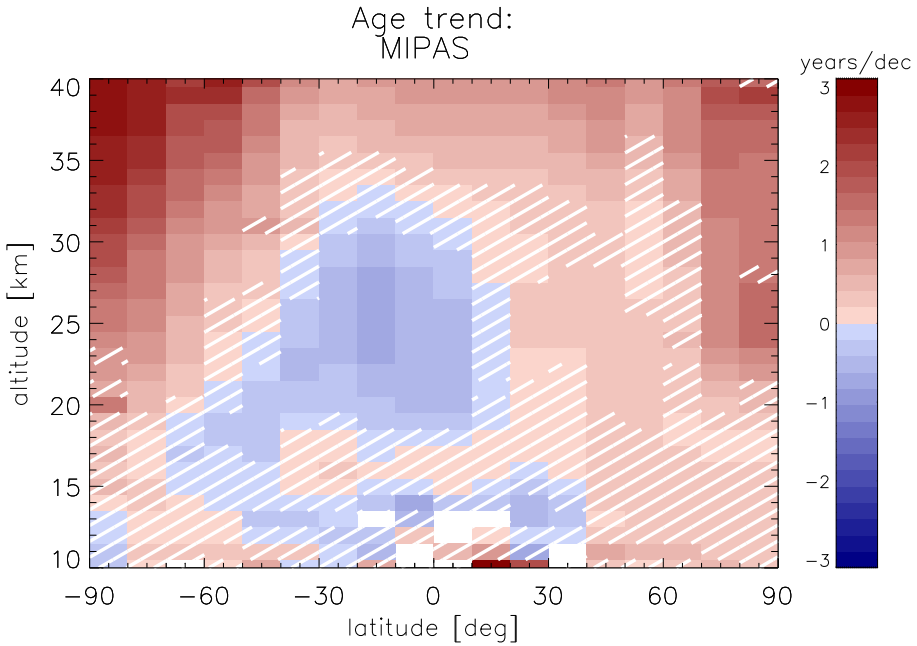

Figure 13. Altitude–latitude cross-section of the AoA model-error corrected linear increase after including the model error and autocorrelations between the data points in the fit. Hatched areas indicate where the trend is not significant.

ACPD
15, 14685–14732, 2015

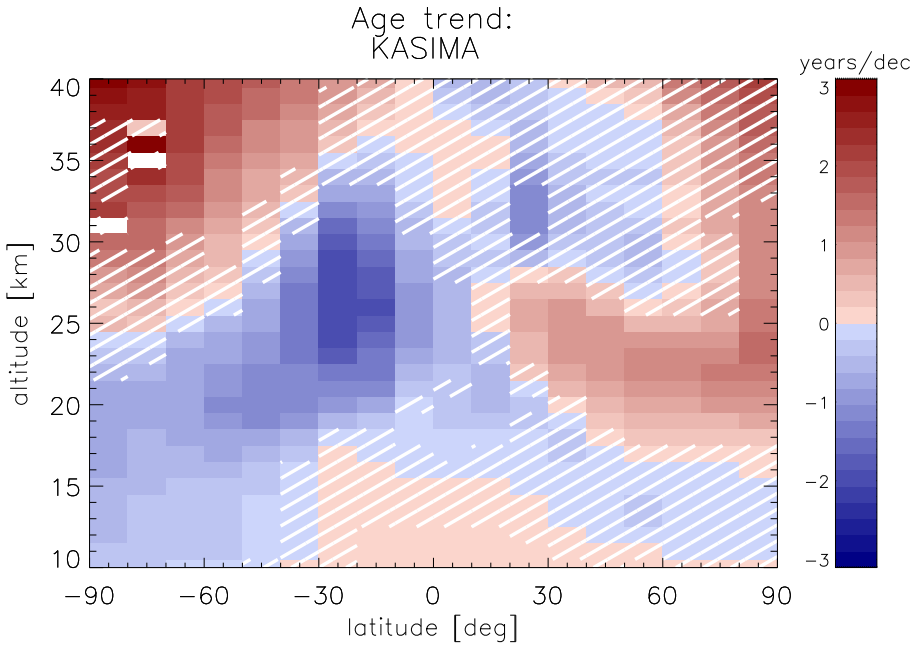

Figure 14. Calculated AoA trends from the KASIMA model with consideration of empirical errors and autocorrelation.

ACPD
15, 14685–14732, 2015